RESOURCE GEOLOGY

doi: 10.1111/j.1751-3928.2012.00185.x *Resource Geology* Vol. 62, No. 2: 140–158

Original Article

The Arinem Te-Bearing Gold-Silver-Base Metal Deposit, West Java, Indonesia

Euis T. YUNINGSIH,[1,4] Hiroharu MATSUEDA,[2] Eko P. SETYARAHARJA[3] and Mega F. ROSANA[4]

[1]*Graduate School of Science,* [2]*The Hokkaido University Museum, Hokkaido University, Sapporo, Japan,* [3]*P.T. Antam Tbk, Jalan Pemuda no.1, Jakarta, Indonesia and* [4]*Faculty of Geology, University of Padjadjaran, Bandung, Indonesia*

Abstract

The vein system in the Arinem area is a gold-silver-base metal deposit of Late Miocene (8.8–9.4 Ma) age located in the southwestern part of Java Island, Indonesia. The mineralization in the area is represented by the Arinem vein with a total length of about 5900 m, with a vertical extent up to 575 m, with other associated veins such as Bantarhuni and Halimun. The Arinem vein is hosted by andesitic tuff, breccia, and lava of the Oligocene–Middle Miocene Jampang Formation (23–11.6 Ma) and overlain unconformably by Pliocene–Pleistocene volcanic rocks composed of andesitic-basaltic tuff, tuff breccia and lavas. The inferred reserve is approximately 2 million tons at 5.7 g t^{-1} gold and 41.5 g t^{-1} silver at a cut-off of 4 g t^{-1} Au, which equates to approximately 12.5t of Au and 91.4t of Ag. The ore mineral assemblage of the Arinem vein consists of sphalerite, galena, chalcopyrite, pyrite, marcasite, and arsenopyrite with small amounts of pyrrhotite, argentite, electrum, bornite, hessite, tetradymite, altaite, petzite, stutzite, hematite, enargite, tennantite, chalcocite, and covellite. These ore minerals occur in quartz with colloform, crustiform, comb, vuggy, massive, brecciated, bladed and calcedonic textures and sulfide veins. A pervasive quartz–illite–pyrite alteration zone encloses the quartz and sulfide veins and is associated with veinlets of quartz–calcite–pyrite. This alteration zone is enveloped by smectite–illite–kaolinite–quartz–pyrite alteration, which grades into a chlorite–smectite–kaolinite–calcite–pyrite zone. Early stage mineralization (stage I) of vuggy–massive–banded crystalline quartz-sulfide was followed by middle stage (stage II) of banded–brecciated–massive sulfide-quartz and then by last stage (stage III) of massive-crystalline barren quartz. The temperature of the mineralization, estimated from fluid inclusion microthermometry in quartz ranges from 157 to 325°C, whereas the temperatures indicated by fluid inclusions from sphalerite and calcite range from 153 to 218 and 140 to 217°C, respectively. The mineralizing fluid is dilute, with a salinity <4.3 wt% NaCl equiv. The ore-mineral assemblage and paragenesis of the Arinem vein is characteristically of a low sulfidation epithermal system with indication of high sulfidation overprinted at stage II. Boiling is probably the main control for the gold solubility and precipitation of gold occurred during cooling in stage I mineralization.

Keywords: Arinem, base metal, fluid inclusion, gold, silver, tellurium.

1. Introduction

The Arinem area is part of the Sunda-Banda magmatic arc that is situated within the Indonesia archipelago at the southern margin of the Sundaland and the Eurasian plates (Carlile & Mitchell, 1994; Corbett & Leach, 1998). Unexploited low-grade gold–silver telluride mineralization at Arinem is an uncommon mineralization assemblage in West Java. The Arinem mineralization, has been regarded as a low-sulfidation epithermal

Received 27 September 2010. Accepted for publication 13 June 2011.
Corresponding author: E. T. YUNINGSIH, Department of Earth and Planetary Sciences, Graduate School of Science, Hokkaido University, Kita-ku, Kita 10 Nishi 8, Sapporo 060-0810, Japan. Email: etintiny@yahoo.com

quartz vein deposit (Antam, 1993). Gold exploration in the Arinem area and its surroundings started in the early 1980s by Antam, the state mining company. Since 1990, detailed exploration, including some drilling activity, has been ongoing to define the gold and base metal reserve, as well as the deposit characteristics.

The main mineralization in the area is the Arinem vein trending N20°W to N10°E for about 5900 m in length. The major zone of economic mineralization in the vein is exposed at an elevation of 365–530 m above sea level and averages 3 to 5 m in width. Initially, anomalies of Au, Ag, Cu, Pb, and Zn were indicated based on stream sediment geochemistry. By applying a cut off grade of 4 g t^{-1} Au, the inferred reserve of ore is 2,204,000 tons or 12.5 tons of Au and 91.4 tons of Ag at an average content of 5.7 g t^{-1} Au and 41.5 g t^{-1} Ag. The gold–silver ratio is approximately 1:10 (Antam, 1993). These reserves result from the Arinem vein and other associated veins, such as the Bantarhuni and Halimun, which occur near the Arinem vein. The deposit is characterized by the high contents of Zn, Pb, and Cu.

The present reserve is projected to result in a relatively short mine life. Thus, the current exploration work is focused on finding additional extensions of the Arinem vein. The exploration is concentrated to the north and south of the main Arinem vein, since the most prospective areas are thought to be both along the strike of the Arinem vein zone, as well as some other veins to the west and east of the Arinem vein.

2. Geological setting

The Arinem area is located in a part of the West Java province, Java Island, Indonesia (Fig. 1). The deposit is situated at the southwest of the Papandayan active volcano and about 200 km southeast of Jakarta. The research area is part of the Southern Mountains of Western Java (Van Bemmelen, 1949; Martodjojo, 1982). The lithology of the area comprises volcanic rocks from the Tertiary to Recent, and consists of tuff breccia as well as undifferentiated old and young volcanic rocks (Fig. 2).

The oldest rock unit is the Jampang Formation which is composed of andesitic tuff, breccias, and lavas. The rocks are commonly altered to propylitic assemblage as a result of a quartz diorite intrusion during Late Oligocene to Middle Miocene age. The Jampang Formation is overlain unconformably by the volcanic rocks of Pliocene age, which is composed of andesitic breccia and tuff. This formation was intruded by Pliocene pyroxene–hornblende andesite. The youngest rocks in the area are volcanic rocks of Pliocene to Pleistocene age that are composed of tuff, tuff breccia, pyroxene andesite and basaltic lavas (Alzwar *et al*., 1992).

3. Analytical method

Thin-, polished- and doubly polished sections of a total of 361 samples were observed using transmitted- and reflected-light microscopes. An additional 23 samples of altered host rocks were investigated by X-ray diffraction analyzer using standard treatment methods for clay mineral identification. The age of mineralization was determined by the K–Ar method at Activation Laboratories Ltd, Ancaster, Ontario, Canada. The K concentration was determined by ICP, and the argon analysis was performed using the isotope dilution procedure on noble gas mass spectrometer. Geochemical analyses for major, minor and trace elements of ores were conducted by ICP at Acme Analytical Laboratories Ltd., Vancouver, Canada.

The compositions of ore minerals were determined using a JEOL 733 electron probe micro analyzer at Hokkaido University. Standards used were natural chalcopyrite, InP, MnS, CdS, FeAsS, Sb_2S_3, PbS, SnS, HgS, ZnS, and elemental Se, Au, Ag, and Te. The probe was operating at 20 kV voltage and the beam current of 10 nA was focused to 1–10 μm diameters with peak counting for 20 s. The X-ray lines measured were As, Se, Te, Cd, Ag, Bi, and Sb (Lα), S, Cu, Zn, Fe, and Mn (Kα), and Pb, Au, and Hg (Mα). The data was corrected by ZAF correction.

Fluid inclusions were examined in 13 samples (11 quartz, 1 sphalerite and 1 calcite). Doubly polished thin sections were prepared at 200 μm thickness. Microthermometric analysis was performed on a Linkam THMSG 600 (Linkam Scientific Instruments, Tadworth, UK) system attached to a Nikon transmitted-light microscope (Nikon Instruments, Melville, NY, USA). Heating rates were maintained near 2°C min^{-1} for measurement of homogenization temperature (Th_{total}) and 0.5°C min^{-1} for measurement of ice melting temperature (Tm). Precision was calculated as ± 0.1°C in the temperature range of the observed phase changes. Accuracy between –60 and –10°C is estimated in the order of ±0.2°C, whereas between –10 and +30°C and above +200°C is placed at ±0.5 and ±2°C, respectively. Instrumental calibration was done using synthetic pure H_2O (0°C), dodecamethylene Glycol (82.0°C), benzanilide (163.0°C), sodium nitrate (306.8°C), n-tridecane (–5.5°C), n-dodecane (–9.6°C), chlorobezene (–45.6°C) and chloroform (–63.4°C) inclusion standards.

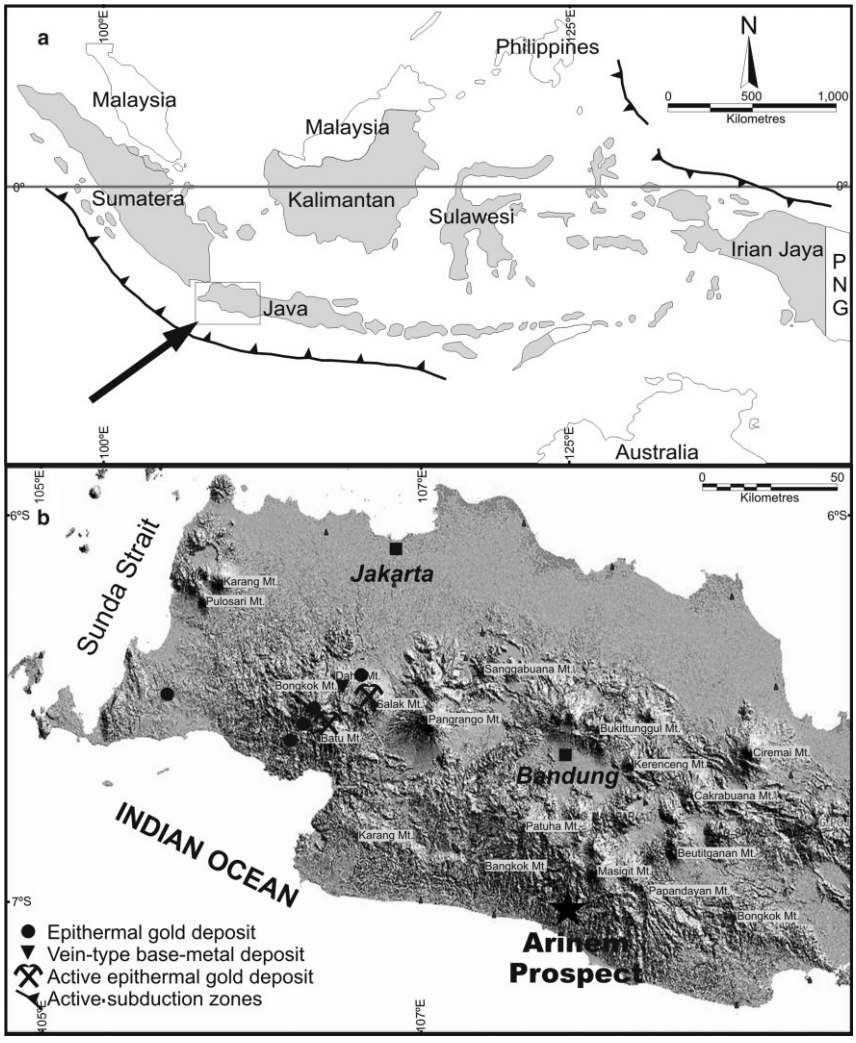

Fig. 1 (a) Map of the Indonesia region, arrow indicates the location of the study area. (b) Geomorphology of western Java with the distributions of active volcanoes and gold deposits. The location of the Arinem deposit is indicated by a black star.

Salinity was determined from the last melting temperatures of ice, utilizing the equation by Bodnar (1993). The possibility of the presence of volatile species (CO_2, N_2), hydrocarbons (CH_4, C_2H_6), and solid phases in fluid inclusions were identified by Raman spectroscopic analyses on limited samples. Analyses were conducted using a JY Horiba T64000 Raman microprobe (JY Horiba, Tokyo, Japan) equipped with an electronically cooled charge-coupled device (CCD) detector, using 514.57 nm (green) Ar-ion laser excitation at Fukuoka University.

4. Geology and structure of Arinem area

Rocks of Tertiary to Recent age occur in the study area and consist of andesitic to basaltic intrusive and extrusive rocks, such as tuff, breccia and lava flows. It is sometimes difficult to distinguish the age of the intrusive and extrusive rocks since the mineralogical composition of those rocks are similar.

The older rocks exposed around the Arinem deposit are andesitic tuff, tuff breccia and aphanitic-porphyritic andesitic lavas. This unit is part of the Late Oligocene to Middle Miocene Jampang Formation (Alzwar *et al*., 1992) which was intruded by phaneritic–porphyritic andesitic rocks. The younger units are andesitic tuff and tuff breccia which are not compacted and are emplaced on the slopes and on the top of the mountain.

There are five major normal faults trending N–S and NE–SW within the research area. Some transverse faults, trending NW–SE and NE–SW, create local

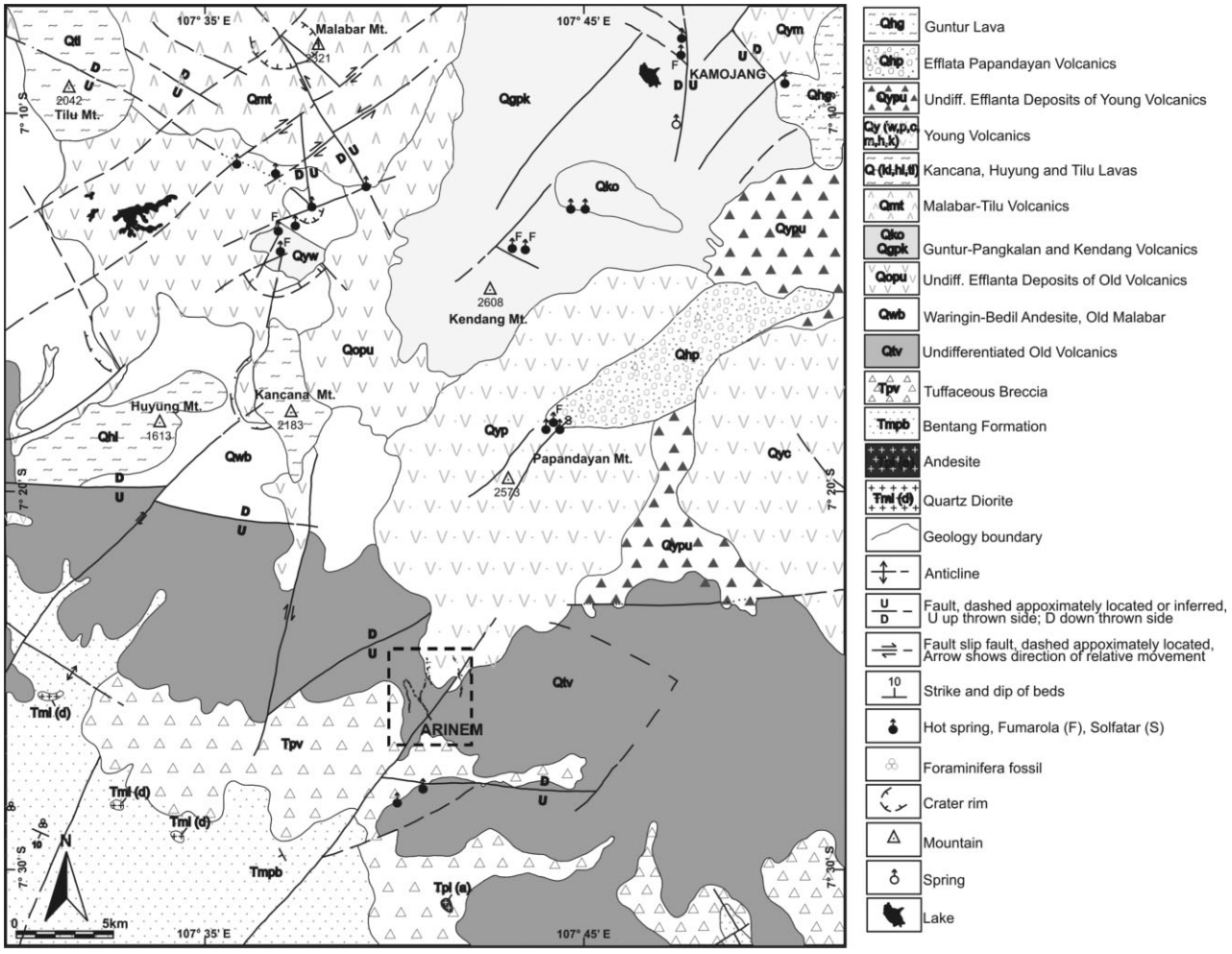

Fig. 2 Regional geological map of the Arinem district and its surrounding (modified after Alzwar *et al*., 1992). Location of the Arinem vein is mark by a dashed-line square.

displacements of the vein zone. The Arinem and Bantarhuni veins occur along Cikandang river and its tributaries such as the Cipanengen and Cibatarua rivers that flow from north to south.

The Bantarhuni quartz vein continues along the Cipanengen river valley at an elevation of 400–450 m above sea level in a N–S direction and with an observed length of around 2300 m. The main Arinem quartz vein is placed along the eastern side of the river with a direction of N20°W to N10°E and dipping around 68–83° westward. The northern part of the vein cuts the Cikandang and Cibatarua rivers. The quartz vein forms an undulating pattern, and its central part was down-faulted in a graben. The Arinem quartz vein forms an extensive braided pattern with lenses of andesitic host-rock.

5. Mineralized system

Among the major veins at Arinem, this study is focused on the mineralization of the main Arinem vein. Most of the data used in this study come from 22 diamond drill holes of an exploration program conducted from 1990 to 2009. The main data come from four diamond drill holes, and these are BCAN 3A (L440m), BCBN 2 (L300m), BCAN 2A (L265m), and BCBN 3 (L200m). These represent the vein at different elevations, such as elevations 440 m, 300 m, 265 m, and 200 m.

The samples taken for analyses came from different elevation and locations in order to represent detailed characteristics of the vein. Though the focus of this research is to analyze core samples from diamond drill

holes, an attempt is made to look beyond the realm of existing bore holes, and to incorporate all existing surface data to understand the mineralization characteristics of the Arinem vein.

5.1 Hydrothermal alteration

The host tuff of the Jampang Formation is composed of volcanic glass, plagioclase, pyroxene, hornblende, and rock fragments of andesitic-basaltic composition. The tuff breccia is composed of andesitic-basaltic fragments, plagioclase, and pyrite in a matrix of tuff. The porphyritic andesitic lava contains abundant plagioclase and pyroxene, together with various amounts of altered hornblende and quartz. Most of the volcanic host rocks such as andesitic tuff, tuff breccia, and lavas have been altered to propylitic and argillic minerals and only a small part is fairly fresh.

Based on the petrographic analyses and additional investigation by X-ray diffraction of drill holes and outcrop samples along the Arinem vein, three alteration zones are recognized:

Silicification (quartz-illite-pyrite) alteration is found within the vein zone and extending into the wall rock with a very small amount of chlorite. The plagioclase phenocrysts in the andesitic rock are completely silicified and altered to illite. Pale-colored chlorite, locally accompanied by calcite, occurs in less silicified rocks. The silicified groundmass consists of mosaic quartz, illite, and disseminated pyrite. Veinlets of quartz + calcite + pyrite are common.

Argillic (smectite-illite-kaolinite-quartz-pyrite) alteration envelops the vein zone and extends up to two meters into the wall rocks above, as well as below, the vein and between orebodies. Most of the primary minerals are found as relicts, altered to hydrothermal minerals. Plagioclase is altered to illite, smectite, and mixed layer illite-smectite, which are in turn variably replaced by calcite. Secondary quartz is abundant in the groundmass and partly forms chalcedony. Kaolinite is present within the hanging-wall shear zone of the vein, in fault crush zones, and along partings within the quartz veins.

Propylitic (chlorite-smectite-kaolinite-calcite-pyrite) alteration is present within the footwall and hanging wall distal to the vein zone. All of the primary phases of the andesitic host rock, except small parts, have been completely replaced. Pyroxene and hornblende phenocrysts are altered to chlorite and calcite. Plagioclase is replaced by illite, smectite, chlorite, and calcite. The groundmass is altered to mixed layered chlorite–smectite, glass in the groundmass is mostly altered to smectite. With increasing intensity of alteration a smectite + mixed layer chlorite-smectite assemblage becomes common.

These alteration types occur throughout the Arinem vein but the extent and intensity of the alteration is closely related to the proximity to quartz veins (Fig. 3). K–Ar ages of 8.8 and 9.4 Ma for illite from altered andesite within the mineralized body were determined (Table 1).

5.2 Mineralization stages

The main Arinem vein is composed predominantly of quartz, calcite, illite and kaolinite, with variable amount of manganese oxide and limonite and with large amounts of sulfides. Colorless, white, pale grey, brownish-reddish white, and brownish-black fine to coarse crystalline quartz are observed, due to the content of accompanied minerals. Colloform, crustiform, comb, vuggy, massive, brecciated, bladed, and calcedonic textures are identified (Fig. 4).

The geochemical analyses show that gold and silver grades vary from 0.09 to 17.5 g t^{-1} Au and from 2.1 to more than 100 g t^{-1} Ag. The base metal contents vary from 0.09 to 11.5% Cu, 0.05 to 22.6% Zn and 0.001 to 15.7% Pb (Table 2).

Based on drill cores observations (see Fig. 5) of the main Arinem vein at the L440m (BCAN 3A), L300m (BCBN 2), L265m (BCAN 2A), and L200m (BCBN 3), the vein was formed in three temporal mineralizing stages. Hand specimen samples, and the paragenesis of ore and gangue mineral varieties of the Arinem vein are shown in Figures 6 and 7. The composition of ores in each stage of mineralization are presented in Table 2. The three stages of mineralization are:

I. *Vuggy-massive-banded crystalline quartz-sulfide*: This stage is considered as the first stage and is divided into four substages of vuggy crystalline quartz (substage IA), massive crystalline quartz-sulfide (substage IB), banded crystalline quartz-sulfide (substage IC), and oxidized massive-crystalline quartz (substage ID). Some vugs between bands of quartz in substages IA and IC are filled with illite, carbonate, and kaolinite. Sphalerite, pyrite, galena, and chalcopyrite are abundant, and subordinate amounts of arsenopyrite, marcasite, electrum, argentite, and pyrrhotite are present in this stage. Covellite,

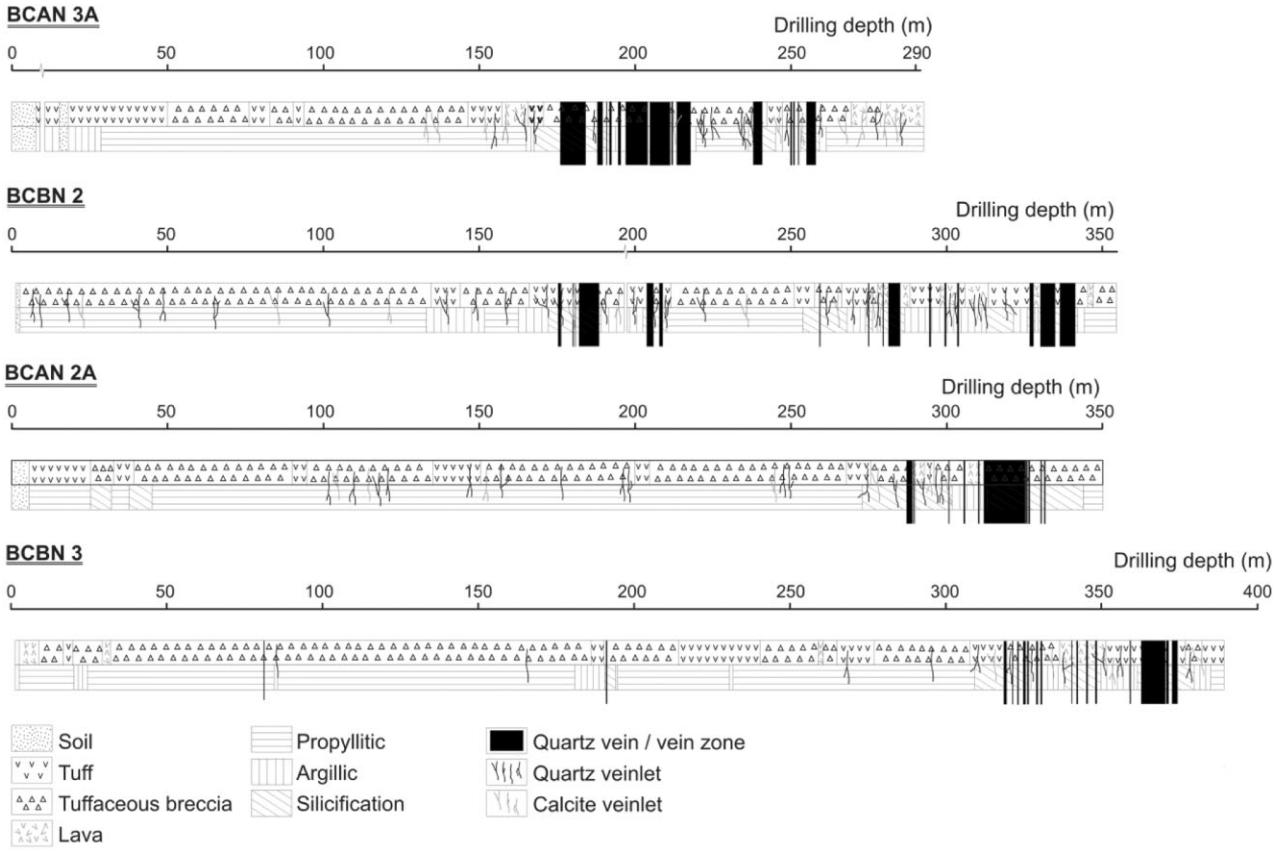

Fig. 3 Host rock type, alteration and the quartz vein of the main mineralization zones from drill core of boreholes BCAN 3A, BCBN 2, BCAN 2A, and BCBN 3 of the Arinem vein.

Table 1 K–Ar age of the mineralized Arinem vein

Sample No.	Sample description	K (%)	$^{40}Ar_{rad}$ (nl g^{-1})	$^{40}Ar_{air}$ (%)	K/Ar Age (Ma)
BCAN 2A-48	illite	1.29	0.466	65.1	9.4 ± 0.3
BCBN 2–75	illite	2.68	0.903	32.4	8.8 ± 0.3

limonite, and manganese oxide are present as alteration products of chalcopyrite and pyrite.

II. *Banded-brecciated-massive sulfide-quartz*: Stage II of the mineralization is represented by banded sulfide-quartz (substage IIA), brecciated sulfide-quartz (substage IIB), and massive sulfide-quartz (substage IIC). In some parts of the vein, the thickness of banded and massive sulfide reaches more than one meter. Ore minerals such as sphalerite, galena, pyrite, and chalcopyrite are more abundant compared to stage I. Other ore minerals are arsenopyrite, marcasite, pyrrhotite, argentite, electrum, and bornite, and the Te-bearing minerals hessite, tetradymite, stutzite, petzite, and altaite. In some samples, the sulfosalt minerals enargite and tennantite have replaced the sulfide minerals chalcopyrite and pyrite. Chalcocite, covellite, and limonite are also found as alteration of chalcopyrite and pyrite. Illite, kaolinite, chlorite, calcite, and smectite are rarely associated with quartz gangue.

III. *Massive-crystalline barren quartz*: This stage consists of abundant quartz, calcite, and small amounts of smectite and illite. This stage is divided

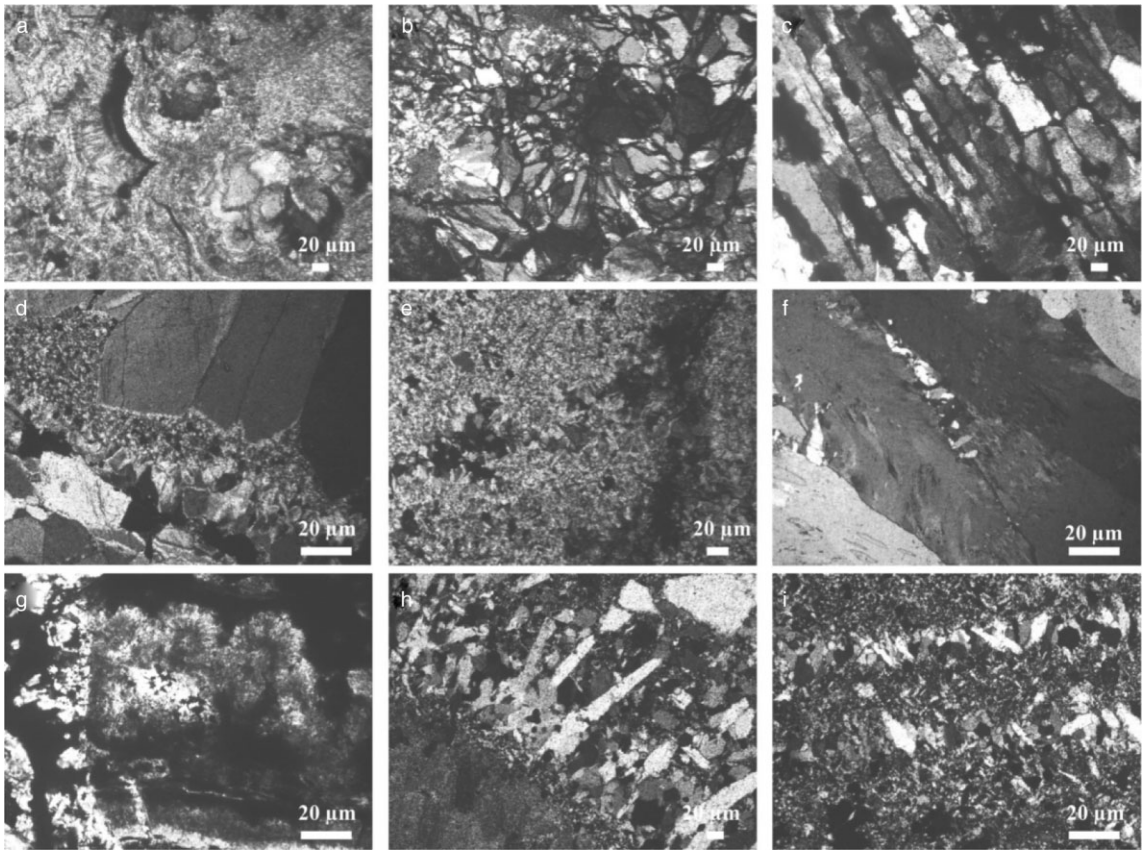

Fig. 4 Transmitted light (crossed nicols) photomicrographs showing the occurrence of various quartz textures. (a) botryoidal form of chalcedony from an outcrop; (b) radial texture of granular quartz, probably pseudomorph after calcite/L440m; (c) bladed/lattice texture of quartz pseudomorph after calcite/L440m; (d) fine-crystalline quartz grown at the end of coarse crystals quartz/L400m; (e) moss textured quartz/L300m; (f) feathered quartz re-crystallization texture/L275m; (g) microcrystalline colloform banded texture associated with clay and ore minerals/L265m; (h) inherited (pseudomorphic) platy structure in replacement lamellar quartz/L265m; (i) millimeter-scale banded texture of microcrystalline quartz intercalated with fine- to medium crystals of quartz/L200m.

into massive barren quartz (substage IIIA) and crystalline barren quartz (substage IIIB). The quartz is characterized by massive, banded, and comb textures with colorless to white-grey yellowish color. Ore minerals are rare in this stage, although pyrite, and a small amount of sphalerite, chalcopyrite, and galena are locally present. This stage is considered to be the last stage of vein formation.

5.3 Ore minerals

The identification of ore mineralogy in the Arinem vein yields some variation. The sulfosalt minerals such as enargite and tennantite replaced the sulfide minerals chalcopyrite and pyrite in late stage II of mineralization associated with hematite. Representative compositions and atomic proportions of sulfides, sulfosalts, and telluride minerals are given in Tables 3–5, respectively. Most data is presented as mean values of every substage of mineralization.

Sphalerite is the dominant sulfide mineral within the Arinem vein and occurs as fine to coarse crystals up to 2 mm in diameter. This mineral occurs in association with galena, pyrite, and chalcopyrite as massive or sulfide-bearing bands in stage II. In stage I, sphalerite is mostly distributed in quartz gangue. Sphalerite contains up to 4.7 wt% Fe and up to 1.1 wt% Cd (Table 3) and locally shows a zonation of Fe from rims to the cores. The composition of sphalerite in stages I and II are relatively homogeneous with FeS contents 0.5–8.5 mol% in stage I and 0.5 to 5.5 mol% in stage II. The

Table 2 Cu, Pb, Zn, Cd, Sb, Bi, Ag, Au, Te, and As contents of the Arinem vein

Substage	Level (m)	Sample No.	Cu (%)	Pb (%)	Zn (%)	Cd (ppm)	Sb (ppm)	Bi (ppm)	Ag (ppm)	Au (ppm)	Te (ppm)	As (ppm)
IA	265	2A-18	0.38	2.85	16.74	1287.3	4.5	11.6	30.3	1.25	32.0	13.2
IB	440	3A-22	0.09	0.31	0.62	47.2	71.2	0.4	35.0	9.10	na	>10,000
IB	300	B.2–47	5.28	1.17	4.81	337.2	23.8	12.9	33.1	2.29	16.0	1158.2
IIA	440	3A-43	1.58	3.42	8.45	587.1	3.4	21.3	60.7	4.15	50.0	45.5
IIA	440	3A-51	0.95	0.39	4.58	363.8	2.8	8.5	45.9	2.01	40.0	207.3
IIA	300	B.2–15	1.11	2.35	7.30	528.7	6.4	18.3	51.4	3.61	53.0	247.8
IIA	300	B.2–16	0.32	3.66	1.48	112.1	8.0	12.7	66.1	2.90	57.0	289.9
IIA	300	B.2–50	11.48	0.03	0.05	2.9	1.2	199.5	>100.0	1.04	156.0	13.6
IIA	265	2A-14.2	0.29	0.001	10.69	1064.7	0.5	0.6	2.1	0.09	2.5	20.6
IIB	440	3A-57	0.51	0.56	3.33	236.8	0.8	5.7	41.6	17.52	38.0	17.1
IIB	440	3A-92	0.33	1.24	2.47	101.7	26.0	0.2	9.7	0.58	14.0	3134.9
IIC	265	2A-22	0.51	15.71	22.63	2000.0	11.9	24.7	>100,0	6.90	209.0	4.4
IIC	265	2A-39.2	0.50	1.32	11.50	885.3	16.3	2.4	12.9	6.97	14.0	1669.8
IIIB	200	B.3–29	0.57	0.20	6.72	487.3	4.3	7.6	22.6	0.17	28.0	155.2
IIIB	200	B.3–81	0.87	0.44	3.02	201.6	22.4	4.5	9.5	0.27	2.5	134.5

na, not analyzed.

intimate association of sphalerite, galena, and chalcopyrite with silver and gold-bearing minerals such as hessite (Ag_2Te), stutzite (Ag_5Te_3), argentite (Ag_2S), petzite (Ag_3AuTe_2), and electrum (Au, Ag) are observed in stage II of mineralization (Fig. 8).

Galena occurs as single crystal or associated with other sulfide minerals up to 5 mm in size in stages I and II. In stage II it contains pyrite, sphalerite, hessite, electrum, and altaite inclusions, but some galena also occurs as inclusions within sphalerite, chalcopyrite, and pyrite.

Chalcopyrite occurs as fine to coarse crystals associated with pyrite and as fine to very fine crystals found as inclusions in galena or as irregular patches. The high Au contents (up to 1.0 wt%) in some chalcopyrite grains is probably due to the distribution of the invisible gold inclusions. Chalcopyrite is commonly found dispersed and as blebs in sphalerite showing chalcopyrite disease texture. Chalcopyrite occurs in most of the ore vein, and is partially replaced by covellite and chalcocite.

Very small grains of *electrum* are found as inclusions in chalcopyrite, galena, and sphalerite with sizes of 2–6 μm in stage II but is rare in stage I. These inclusions appear to be co-depositional with the host sulfides, which are fine- to medium-crystalline (~1.0 mm) based on textural evidence. Electrum crystals are too small for further analyses by microprobe.

Silver minerals observed under the microscope are very small grains of argentite and telluride such as hessite, stutzite, and petzite in stage II. The silver content in hessite minerals ranges from 64.6–67.1 wt%, in the stutzite between 60.7–61.0 wt%, and in petzite is 47.9–52.7 wt%.

Telluride minerals including hessite, tetradymite, stutzite, petzite, and altaite are present in the stage II mineral assemblage of the mineralized vein. Hessite is the most abundant telluride mineral in the deposit. Some hessite grains coexist with tetradymite as inclusions in chalcopyrite. Petzite associated with hessite is found as inclusions in sphalerite and galena, mostly as irregular patches up to 10 μm in diameter. Some grains of hessite contain Au up to 3.5 wt%. Au and Ag contents of petzite range between 14.2 to 18.3 wt% and 48.0 to 52.7 wt%, respectively. Tetradymite is generally 5–20 μm in size, occurs together with hessite, and is commonly observed as isolated grains and inclusions in chalcopyrite. Tetradymite contains up to 0.5 wt% Ag, 0.4 wt% Au and 1.3 wt% Se. Altaite is the sole Pb-telluride observed in the Arinem vein and contains up to 32.5 wt% Te, 0.7 wt% Ag and 0.6 wt% Au.

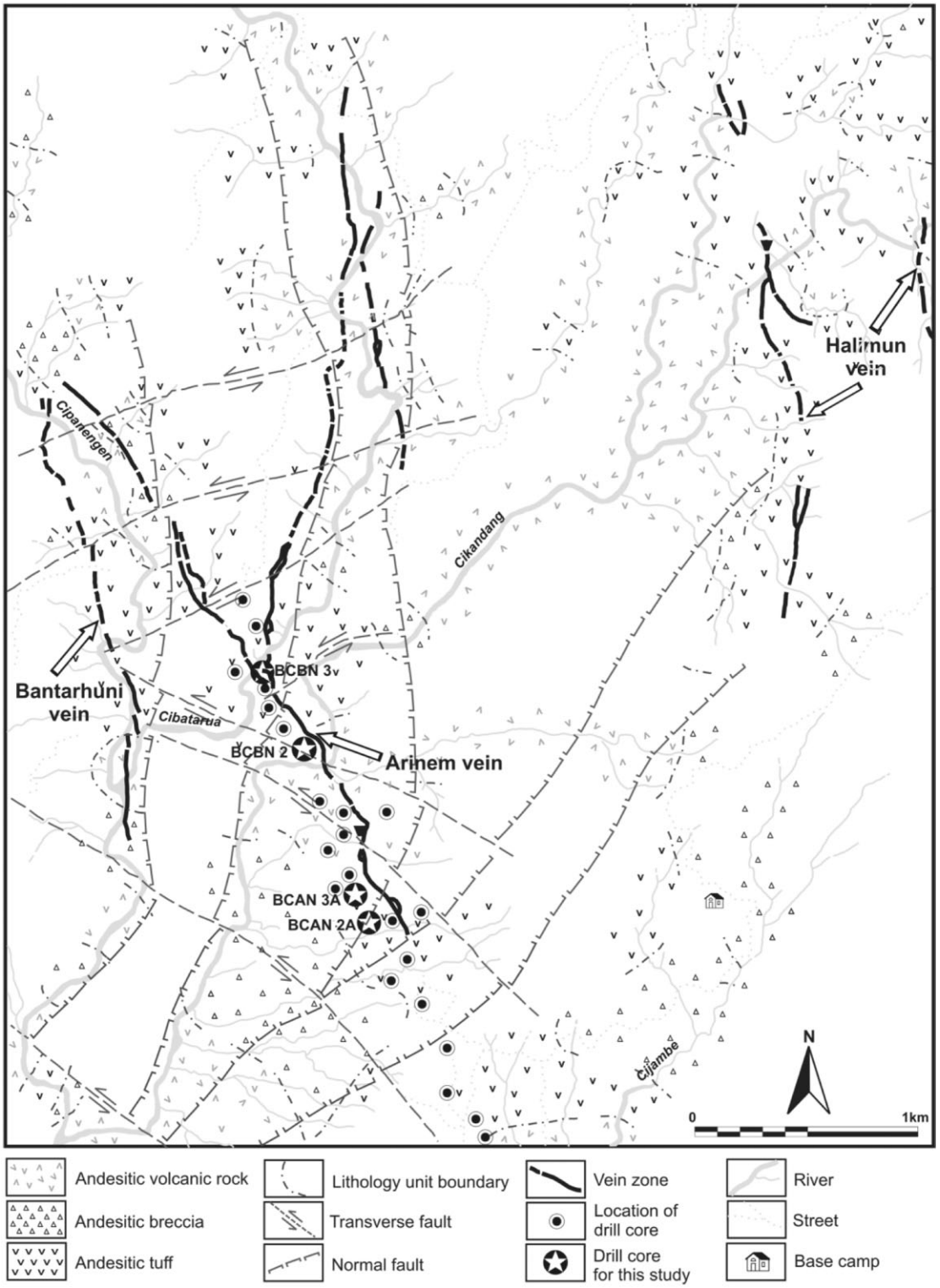

Fig. 5 Geology and structural map of the Arinem deposit, West Java, Indonesia. The location of the Bantarhuni and Halimun veins are indicated west and east of the Arinem vein (modified after Antam, 1993).

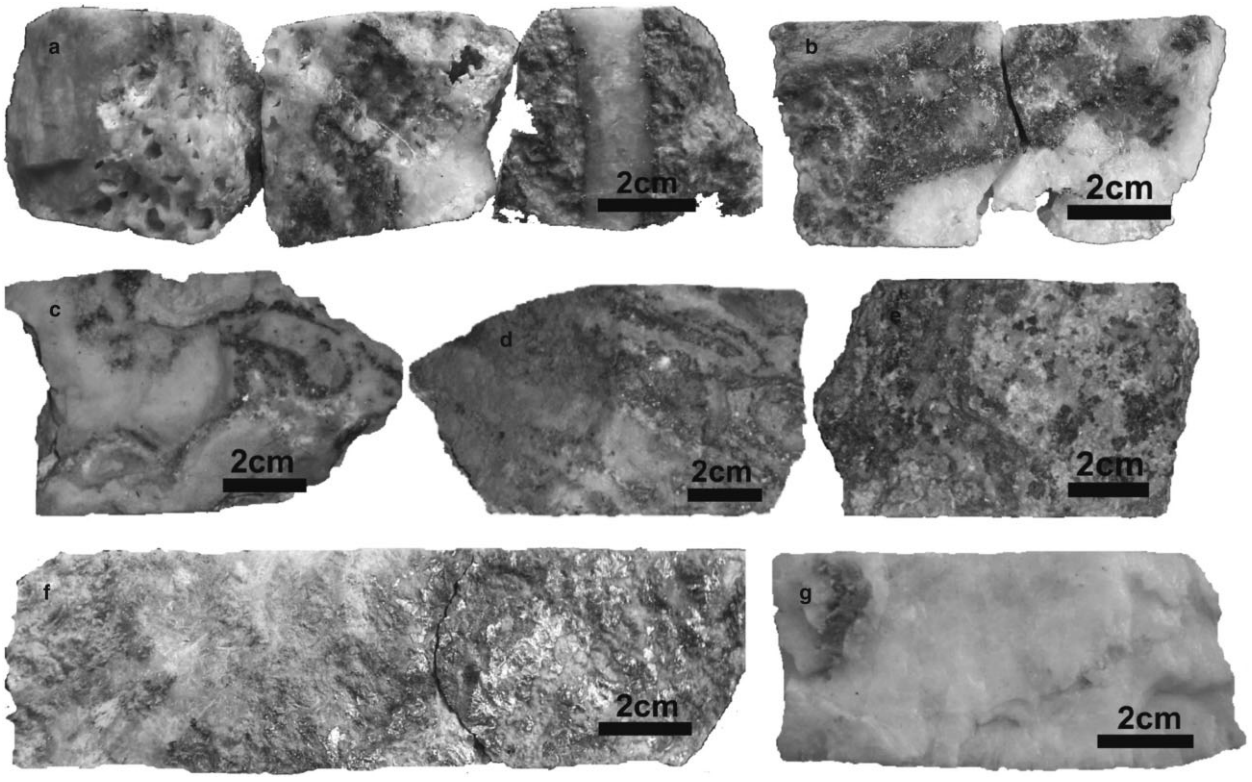

Fig. 6 Hand specimens of the Arinem vein from core samples. (a) chalcedony and crystalline quartz of substage IIIB cut vuggy quartz of substage IA/L425m; (b) crystalline quartz-sulfide of substage IB L^{-1}-60 m; (c) banded quartz-sulfide of substage IC/L440m; (d) banded sulfide-quartz of substage IIA/L440m; (e) banded sulfide-quartz associated with white clay minerals and pale brownish carbonate of substage IIA/L440m; (f) massive chalcopyrite, pyrite, sphalerite and galena of substage IIC/L300m; (g) massive barren milky quartz of substage IIIA/L300m.

Characteristic X-ray energy-dispersive and back scattered electron images of the coexisting occurrences of hessite with tetradymite and petzite are shown in Figure 9.

Other minerals such as marcasite, pyrrhotite, arsenopyrite, and bornite occur as minor and trace ore minerals. Some pyrrhotite grains are replaced by pyrite and/or marcasite in stages I and II. As contents of pyrite is up to 0.3 wt% and Au up to 0.7 wt%. Arsenopyrite displays prominent compositional zonation with Sb contents of up to 0.6 wt%. Sulfosalt minerals of tennantite and enargite of late stage II mineralization characterized by As contents 10.7 to 18.0 wt% and Sb is up to 6.8 wt%. The iron content in enargite is up to 17.0 wt%.

The near-surface levels of the Arinem vein are extensively oxidized and patches of complete oxidation extend to depths of 250 m. The ore composition in the oxidation zone is dominated by iron oxyhydroxides, manganese oxides, with minor goethite, chalcocite, and covellite in the transition zone to the partially oxidized sulfide veins.

5.4 Fluid inclusions

Microthermometric study was carried out on the quartz, sphalerite, and calcite samples from the Arinem vein from different levels and stages of mineralization. The inclusions observed were large enough to study aqueous inclusions, mostly consisting of two phases liquid (L) and vapor (V) at room temperature. The L–V inclusions are dominant in most inclusions (avg > 70 vol%). However, vapor bubbles occupy up to ~90 vol% in some of the inclusions. The L–V inclusions occur in clear, smoky, and milky quartz, medium- and coarse-crystalline calcite, and in sphalerite of substage IIA (Fig. 10). Some of the fluid inclusions were necked down. The fluid inclusions used in the microthermometric study ranged from 5 to 40 μm in diameter.

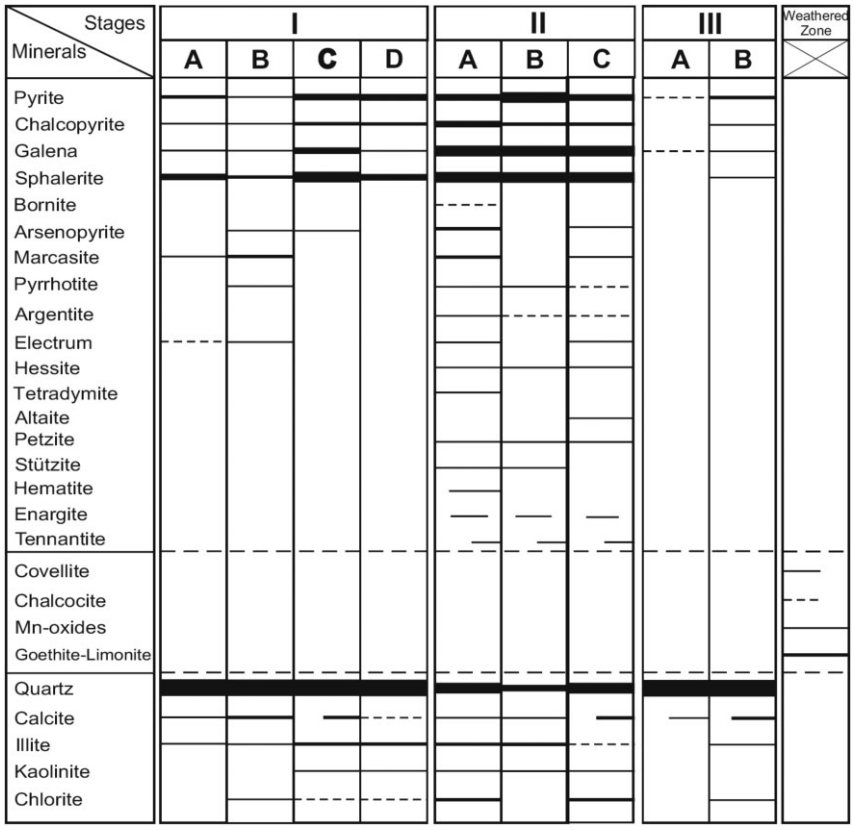

Fig. 7 Paragenesis of ore and gangue minerals of the Arinem vein. Width of bars corresponds to the relative abundance of each mineral.

The inclusions which occur in clusters or isolated within the crystals are regarded as "primary", and others in planar arrays outlining growth zones or in healed fractures that terminated against growth zones are considered as "pseudo-secondary" in this study. Inclusions in quartz and sphalerite that occur in planes of healed fractures that do not terminate against growth zones were considered secondary, as these fractures commonly cut across crystal boundaries. Secondary fluid inclusions are less than 20 μm in diameter. Three types of fluid inclusion are recognized. Those are: (i) two-phase primary and pseudo-secondary liquid-rich fluid inclusions; (ii) two-phase primary and pseudo-secondary vapor-rich fluid inclusions; and (iii) two-phase secondary liquid-rich fluid inclusions.

The results of measurements from the primary fluid inclusions in quartz from different levels indicate that the homogenization temperature of stage I is in the range of 177–325°C, of stage II is 157–312°C, and of stage III is 165–236°C. Measurements from sphalerite and calcite from substages IIA and IIIB give results of 153–218°C and 140–217°C, respectively. Bladed quartz texture was observed in the stage I Arinem vein, but the vapor-rich inclusions were not observed in bladed quartz. Quartz samples of substage IA contain both gas-rich and liquid-rich inclusions along the same growth band. The filling temperatures of these two types of fluid inclusion range from 217 to 247°C. Sphalerite samples also contained vapor-rich inclusions but some were interpreted to have formed by necking down.

The salinities of the fluid inclusions in quartz, sphalerite, and calcite are less than 4.3 wt% NaCl equiv. The salinity determined on quartz is, on average, 1.9 wt% NaCl equiv., 2.6 wt% NaCl equiv. on sphalerite, and 2.1 wt% NaCl equiv. on calcite. The ranges of homogenization temperature and salinity from fluid inclusions of stages I to III are presented in Figure 11. Raman spectroscopic analyses performed on selected fluid inclusions detected no volatile components other than H_2O.

6. Discussion

The data obtained by this study shows that the Arinem deposit is a quartz–illite–calcite–sulfide vein, which

Table 3 Representative chemical composition of sulfide minerals

		(wt %)																Total
		Zn	Cu	Fe	Mn	S	Ag	Cd	As	Se	In	Sb	Pb	Au	Te	Hg	Bi	
Sphalerite																		
Substage IA	Mean ($N = 16$)	63.54	0.05	1.12	0.07	32.49	0.06	0.27	<0.01	<0.01	<0.01	<0.01	<0.01	0.07	<0.01	na	na	97.67
Substage IB	Mean ($N = 35$)	63.67	0.32	1.11	0.04	32.71	0.03	0.45	0.11	<0.01	na	0.01	<0.01	0.02	<0.01	<0.01	0.01	98.48
Substage IC	Mean ($N = 10$)	65.07	0.06	1.04	0.11	32.70	0.02	0.26	<0.01	<0.01	0.01	0.03	na	na	na	na	na	99.31
Substage IIA	Mean ($N = 38$)	63.69	0.09	1.02	0.06	32.06	0.03	0.46	0.07	0.01	<0.01	<0.01	0.01	0.06	<0.01	na	na	97.57
Substage IIB	Mean ($N = 17$)	64.19	0.06	0.65	0.01	32.77	0.03	0.25	0.03	<0.01	<0.01	<0.01	0.01	0.04	0.01	<0.01	<0.01	98.04
Substage IIC	Mean ($N = 21$)	63.87	0.14	1.16	0.08	32.69	0.03	0.35	<0.01	<0.01	0.01	0.01	<0.01	0.01	0.01	0.03	na	98.38
Substage IIIB	Mean ($N = 27$)	64.36	0.11	0.92	0.09	32.61	0.02	0.42	0.01	<0.01	0.02	0.01	na	na	na	<0.01	na	98.57
	Mean ($N = 164$)	**63.94**	**0.14**	**1.01**	**0.06**	**32.53**	**0.03**	**0.38**	**0.04**	**<0.01**	**0.01**	**0.01**	**<0.01**	**0.03**	**<0.01**	**<0.01**	**<0.01**	**98.20**
	Atomic prop.	***0.97***	***0.00***	***0.02***	***0.00***	***1.00***	***0.00***	***0.00***	***0.00***	***0.00***	***0.00***	***0.00***	***0.00***	***0.00***	***0.00***	***0.00***	***0.00***	
Pyrite																		
Substage IC	$N = 1$	0.01	0.01	47.37	<0.01	53.45	<0.01	0.25	<0.01	<0.01	<0.01	0.03	na	na	na	na	na	101.12
Substage IIA	Mean ($N = 7$)	0.06	0.58	46.84	0.01	52.91	0.02	0.06	0.04	<0.01	<0.01	0.02	0.03	0.15	0.00	0.04	na	100.76
Substage IIB	$N = 1$	<0.01	<0.01	46.59	0.01	53.85	0.06	0.01	<0.01	<0.01	<0.01	<0.01	0.06	<0.01	<0.01	<0.01	na	100.58
Substage IIC	Mean ($N = 6$)	0.05	0.03	47.42	0.01	53.56	0.01	0.03	0.06	<0.01	0.02	na	na	na	na	na	na	101.19
Substage IIIB	Mean ($N = 3$)	0.13	0.19	47.05	0.01	53.41	<0.01	0.12	0.01	<0.01	<0.01	na	na	na	na	na	na	100.92
	Mean ($N = 18$)	**0.06**	**0.27**	**47.08**	**0.01**	**53.29**	**0.02**	**0.07**	**0.04**	**<0.01**	**0.01**	**0.01**	**0.02**	**0.06**	**<0.01**	**0.01**	**na**	**100.94**
	Atomic prop.	***0.00***	***0.01***	***1.00***	***0.00***	***1.99***	***0.00***	***0.00***	***0.00***	***0.00***	***0.00***	***0.00***	***0.00***	***0.00***	***0.00***	***0.00***	***na***	
Marcasite																		
Substage IB	Mean ($N = 8$)	0.01	0.05	46.69	<0.01	54.10	0.04	0.05	0.01	<0.01	na	0.04	0.10	0.08	<0.01	0.05	<0.01	101.23
Substage IIC	Mean ($N = 3$)	<0.01	0.55	46.49	0.01	54.10	0.04	0.01	<0.01	<0.01	na	0.04	<0.01	0.07	0.02	<0.01	0.05	101.40
	Mean ($N = 11$)	**0.01**	**0.19**	**46.64**	**<0.01**	**54.10**	**0.04**	**0.04**	**0.01**	**<0.01**	**na**	**0.04**	**0.07**	**0.08**	**0.01**	**0.04**	**0.01**	**101.27**
	Atomic prop.	***0.00***	***0.00***	***0.99***	***0.00***	***2.00***	***0.00***	***0.00***	***0.00***	***0.00***	**na**	***0.00***	***0.00***	***0.00***	***0.00***	***0.00***	***0.00***	
Arsenopyrite																		
Substage IB	Mean ($N = 5$)	<0.01	0.02	36.74	0.01	20.82	0.01	0.02	42.48	<0.01	na	0.17	0.12	0.02	0.08	<0.01	<0.01	100.50
Substage IIA	Mean ($N = 5$)	0.01	0.03	36.03	<0.01	21.07	0.03	0.01	42.82	<0.01	na	0.35	0.09	0.19	na	0.05	na	100.69
	Mean ($N = 10$)	**0.01**	**0.03**	**36.38**	**0.01**	**20.95**	**0.02**	**0.02**	**42.65**	**<0.01**	**na**	**0.26**	**0.11**	**0.11**	**0.04**	**0.02**	**<0.01**	**100.60**
	Atomic prop.	***0.00***	***0.00***	***1.04***	***0.00***	***1.05***	***0.00***	***0.00***	***0.91***	***0.00***	**na**	***0.00***	***0.00***	***0.00***	***0.00***	***0.00***	***0.00***	
Chalcopyrite																		
Substage IA	Mean ($N = 4$)	0.30	34.03	30.69	na	33.26	0.03	<0.01	<0.01	<0.01	na	<0.01	0.04	0.01	<0.01	na	na	98.35
Substage IB	Mean ($N = 13$)	0.01	34.12	31.20	<0.01	33.93	0.02	0.04	<0.01	<0.01	na	<0.01	<0.01	<0.01	<0.01	na	na	99.33
Substage IC	$N = 1$	0.05	34.25	31.10	<0.01	34.49	<0.01	<0.01	<0.01	<0.01	<0.01	<0.01	na	na	na	na	na	99.89
Substage IIA	Mean ($N = 5$)	0.02	34.15	31.01	0.06	33.92	0.04	0.01	0.01	<0.01	<0.01	<0.01	0.03	0.19	<0.01	0.08	na	99.53
Substage IIB	Mean ($N = 7$)	0.35	33.66	30.33	<0.01	33.44	0.06	0.01	<0.01	<0.01	<0.01	<0.01	0.01	0.01	<0.01	na	na	97.87
Substage IIC	Mean ($N = 12$)	0.05	34.19	30.89	<0.01	34.28	0.04	0.04	<0.01	<0.01	<0.01	<0.01	0.02	0.08	<0.01	0.04	na	99.63
Substage IIIB	Mean ($N = 3$)	<0.01	29.92	32.90	<0.01	36.95	0.03	<0.01	<0.01	<0.01	0.01	<0.01	<0.01	<0.01	<0.01	na	na	99.82
	Mean ($N = 45$)	**0.08**	**33.78**	**31.03**	**0.01**	**34.10**	**0.04**	**0.02**	**<0.01**	**<0.01**	**<0.01**	**<0.01**	**0.01**	**0.05**	**<0.01**	**0.02**	**na**	**99.14**
	Atomic prop.	***0.00***	***0.97***	***1.01***	***0.00***	***1.93***	***0.00***	***0.00***	***0.00***	***0.00***	***0.00***	***0.00***	***0.00***	***0.00***	***0.00***	***0.00***	**na**	
Galena																		
Substage IA	Mean ($N = 4$)	<0.01	<0.01	0.10	<0.01	16.16	0.03	0.03	<0.01	<0.01	na	na	85.09	<0.01	0.03	na	na	101.45
Substage IB	$N = 1$	0.03	0.35	0.24	<0.01	13.52	<0.01	0.03	<0.01	<0.01	na	<0.01	86.45	<0.01	0.08	na	na	100.71
Substage IC	Mean ($N = 3$)	0.63	0.21	0.35	0.01	13.88	<0.01	0.10	<0.01	<0.01	0.02	0.01	85.59	na	<0.01	na	na	100.81
Substage IIA	Mean ($N = 17$)	0.13	0.01	0.38	<0.01	15.18	0.02	0.08	0.32	0.01	<0.01	0.01	84.93	<0.01	0.04	0.03	na	101.15
Substage IIB	Mean ($N = 9$)	0.04	0.01	0.12	<0.01	15.73	0.01	0.03	0.12	0.01	na	0.02	85.09	0.02	0.06	<0.01	na	101.27
Substage IIC	Mean ($N = 2$)	0.01	<0.01	0.10	<0.01	13.22	<0.01	0.05	<0.01	<0.01	na	<0.01	86.75	0.10	0.05	0.14	na	100.42
Substage IIIB	$N = 1$	<0.01	<0.01	0.04	<0.01	13.02	<0.01	0.06	<0.01	<0.01	0.08	na	85.20	<0.01	<0.01	na	na	98.40
	Mean ($N = 37$)	**0.12**	**0.03**	**0.26**	**<0.01**	**15.10**	**0.01**	**0.06**	**0.17**	**0.01**	**0.01**	**0.01**	**85.19**	**0.01**	**0.04**	**0.02**	**na**	**101.06**
	Atomic prop.	***0.01***	***0.00***	***0.01***	***0.00***	***1.06***	***0.00***	***0.00***	***0.00***	***0.00***	***0.00***	***0.00***	***0.92***	***0.00***	***0.00***	***0.00***	**na**	

na, not analyzed.

Table 4 Representative chemical composition of enargite and tennantite

		(wt %)													Total
		Zn	Cu	Fe	Mn	S	Ag	Cd	As	Se	Sb	Pb	Au	Te	Hg	
Enargite																
Substage IIB	$N = 2$	*<0.01*	*47.30*	*1.63*	*<0.01*	*33.33*	*<0.01*	*0.02*	*18.03*	*<0.01*	*0.14*	*0.03*	*<0.01*	*<0.01*	*<0.01*	100.49
		0.03	*44.32*	*3.84*	*0.03*	*33.29*	*<0.01*	*<0.01*	*15.43*	*<0.01*	*2.06*	*<0.01*	*0.21*	*<0.01*	*0.42*	99.61
Substage IIC	$N = 1$	*<0.01*	*48.12*	*0.80*	*0.03*	*32.80*	*0.04*	*0.05*	*17.55*	*<0.01*	*0.47*	*<0.01*	*<0.01*	*<0.01*	*<0.01*	99.84
	Mean ($N = 3$)	**0.01**	**46.58**	**2.09**	**0.02**	**33.14**	**0.01**	**0.03**	**17.00**	**<0.01**	**0.89**	**0.01**	**0.07**	**<0.01**	**0.14**	**99.98**
	***Atomic prop.*[1)]**	***0.00***	***2.90***	***0.11***	***0.00***	***4.03***	***0.00***	***0.00***	***0.92***	***0.00***	***0.03***	***0.00***	***0.00***	***0.00***	***0.00***	
Tennantite																
Substage IIC	$N = 1$	**1.79**	**46.68**	**1.42**	**0.01**	**27.88**	**0.09**	**0.30**	**14.51**	**0.00**	**6.84**	**<0.01**	**<0.01**	**<0.01**	**0.17**	**99.69**
	***Atomic prop.*[2)]**	***0.11***	***2.88***	***0.10***	***0.00***	***3.20***	***0.00***	***0.01***	***0.73***	***0.00***	***0.22***	***0.00***	***0.00***	***0.00***	***0.00***	

na, not analyzed; on the basis of [1)]8 a.p.f.u; [2)]7.25 a.p.f.u.

occurs along fault planes in Oligocene–Miocene volcanic rocks. Based on the fluid inclusion data, the average value of the fluid temperatures during stages I and II mineralization is considered to have been between 194 and 267°C, with a salinity less than 4.3 wt% NaCl equiv. The limited variation in salinity in all samples suggest that the quartz samples grew from fluids with a constant salinity with time (Alderton & Fallick, 2000).

Fluid inclusions data from quartz samples also show that the Arinem vein indicates a systematic decrease of average temperature from stage I to stage III mineralization. The average temperature of stage I is 267 to 219°C (L200m to L440m), stage II of 247 to 203°C (L200m to L440m) and stage III of 194°C (L265m).

Gold and silver content in the Arinem vein varies greatly. At depth, Au and Ag anomalies are related to higher contents of base metal and its distributions at the highest levels are in a wider range. Individual mineral analyses for the elements indicate that As and Sb are highly concentrated in the arsenopyrite of stages I to II, and also in the later stage II of enargite and tennantite.

The ore mineral variation in the Arinem vein could be used as a guide to ore depositional conditions. This study demonstrates an occurrence of precious metal tellurides in the Arinem deposit. The occurrence of Te-bearing minerals such as hessite, tetradymite, stutzite, petzite, and altaite observed in the mineralization stage II point to some activity of the Te-rich fluid in the system. The presence of arsenopyrite and pyrrhotite in stages I and II are characteristic of low sulfidation state epithermal deposits. By contrast, the replacement of Cu–As minerals of enargite and tennantite in late stage II mineralization is a common characteristic of high sulfidation states. These differences reflect the distinct change of redox conditions of the hydrothermal fluids.

The presence of chlorite/smectite and illite/smectite mixed layer minerals indicate a near-neutral pH during mineralization (Hedenquist *et al*., 1996). However, the presence of kaolinite in the argillic and propyllitic alteration assemblages within the vein probably formed during initial leaching of the acid-altered rocks. Alternatively, the kaolinite formed during secondary, supergene processes related to the penetration of meteoric water into permeable fault zones. This process was also associated with the formation of abundant limonite throughout the vein, from the supergene oxidation of sulfides (pyrite and chalcopyrite). K/Ar-dating of illite from altered andesite wall rocks adjacent to the mineralized vein yielded a Late Miocene age (8.8 and

Table 5 Representative chemical composition of hessite, petzite, stutzite, altaite, and tetradymite

		(wt %)															
		Zn	Cu	Fe	Mn	S	Ag	Cd	As	Se	Sb	Pb	Au	Te	Hg	Bi	Total
Hessite																	
Substage IIA	Mean ($N = 9$)	0.15	0.24	0.16	<0.01	0.08	61.96	0.10	<0.01	<0.01	<0.01	0.16	0.17	35.28	0.08	na	98.38
Substage IIB	Mean ($N = 3$)	0.48	0.07	0.16	0.03	0.30	61.89	0.20	<0.01	<0.01	<0.01	<0.01	1.77	33.65	0.32	na	98.85
Substage IIC	Mean ($N = 3$)	0.46	0.01	0.01	<0.01	0.07	62.30	0.10	<0.01	<0.01	<0.01	0.59	0.07	35.39	0.08	na	99.06
	Mean ($N = 15$)	**0.27**	**0.16**	**0.13**	**0.01**	**0.12**	**62.01**	**0.12**	**<0.01**	**<0.01**	**<0.01**	**0.22**	**0.47**	**34.98**	**0.13**	**na**	**98.62**
	***Atomic prop.*[1)]**	***0.01***	***0.01***	***0.01***	***0.00***	***0.01***	***1.98***	***0.00***	***0.00***	***0.00***	***0.00***	***0.00***	***0.01***	***0.97***	***0.00***	**na**	
Petzite																	
Substage IIA	$N = 2$	0.01	0.17	0.09	<0.01	0.12	51.36	0.05	<0.01	<0.01	<0.01	0.13	14.32	32.55	<0.01	na	98.80
		<0.01	0.28	0.51	<0.01	0.03	52.74	0.11	<0.01	<0.01	<0.01	<0.01	15.54	30.83	0.04	na	100.08
Substage IIB	$N = 1$	0.13	<0.01	0.03	0.02	0.36	49.25	0.11	<0.01	<0.01	<0.01	0.06	14.24	34.89	0.22	na	99.30
Substage IIC	$N = 2$	0.25	<0.01	<0.01	<0.01	0.10	47.96	0.02	<0.01	<0.01	<0.01	0.11	18.32	34.24	<0.01	na	101.00
		1.32	0.04	0.02	<0.01	0.12	49.79	0.07	<0.01	<0.01	<0.01	<0.01	15.03	32.88	<0.01	na	99.26
	Mean ($N = 5$)	**0.34**	**0.10**	**0.13**	**<0.01**	**0.15**	**50.22**	**0.07**	**<0.01**	**<0.01**	**<0.01**	**0.06**	**15.49**	**33.08**	**0.05**	**na**	**99.68**
	***Atomic prop.*[2)]**	***0.06***	***0.01***	***0.02***	***0.00***	***0.03***	***3.17***	***0.01***	***0.00***	***0.00***	***0.00***	***0.00***	***0.68***	***2.01***	***0.00***	**na**	
Stutzite																	
Substage IIA	$N = 2$	<0.01	<0.01	<0.01	<0.01	0.03	60.67	0.08	<0.01	<0.01	<0.01	<0.01	<0.01	37.13	0.25	0.24	98.40
		0.17	0.07	0.06	<0.01	0.04	61.03	<0.01	<0.01	<0.01	<0.01	0.83	0.14	36.68	0.20	<0.01	99.21
Substage IIB	$N = 1$	0.05	0.02	<0.01	0.02	0.07	61.05	<0.01	<0.01	<0.01	<0.01	<0.01	0.19	41.70	0.30	na	103.41
	Mean ($N = 3$)	**0.07**	**0.03**	**0.02**	**0.01**	**0.05**	**60.91**	**0.03**	**<0.01**	**<0.01**	**<0.01**	**0.28**	**0.11**	**38.51**	**0.25**	**0.08**	**100.26**
	***Atomic prop.*[3)]**	***0.03***	***0.00***	***0.00***	***0.00***	***0.01***	***5.12***	***0.00***	***0.00***	***0.00***	***0.00***	***0.00***	***0.01***	***2.80***	***0.01***	***0.00***	
Altaite																	
Substage IIC	$N = 1$	<0.01	<0.01	0.05	0.01	0.31	0.67	0.05	<0.01	<0.01	<0.01	63.04	0.55	32.45	0.52	<0.01	97.65
	Atomic prop.[4)]	**0.00**	**0.00**	**0.00**	**0.00**	**0.03**	**0.00**	**0.00**	**0.00**	**0.00**	**0.00**	**1.00**	**0.01**	**0.93**	**0.01**	**0.00**	
Tetradymite																	
Substage IIA	$N = 4$	0.02	0.13	0.09	0.03	3.82	0.17	<0.01	<0.01	0.74	<0.01	<0.01	<0.01	34.81	<0.01	58.08	97.88
		<0.01	0.94	0.66	<0.01	4.26	0.48	0.02	<0.01	0.08	<0.01	<0.01	0.13	34.81	<0.01	57.76	99.14
		<0.01	0.32	0.31	0.02	3.76	0.21	<0.01	<0.01	0.65	<0.01	<0.01	0.08	35.79	0.59	55.70	97.43
		0.03	0.04	0.77	<0.01	3.12	0.13	<0.01	<0.01	1.31	<0.01	<0.01	0.39	35.60	0.10	57.47	98.95
	Mean ($N = 4$)	**0.01**	**0.36**	**0.46**	**0.01**	**3.74**	**0.25**	**0.01**	**<0.01**	**0.69**	**<0.01**	**<0.01**	**0.15**	**35.25**	**0.17**	**57.25**	**98.35**
	***Atomic prop.*[5)]**	***0.00***	***0.03***	***0.04***	***0.00***	***0.95***	***0.02***	***0.00***	***0.00***	***0.06***	***0.00***	***0.00***	***0.01***	***1.95***	***0.01***	***1.93***	

na, no analyzed; on the basis of [1)]3 a.p.f.u; [2)]6 a.p.f.u; [3)]8 a.p.f.u; [4)]2 a.p.f.u; [5)]5 a.p.f.u.

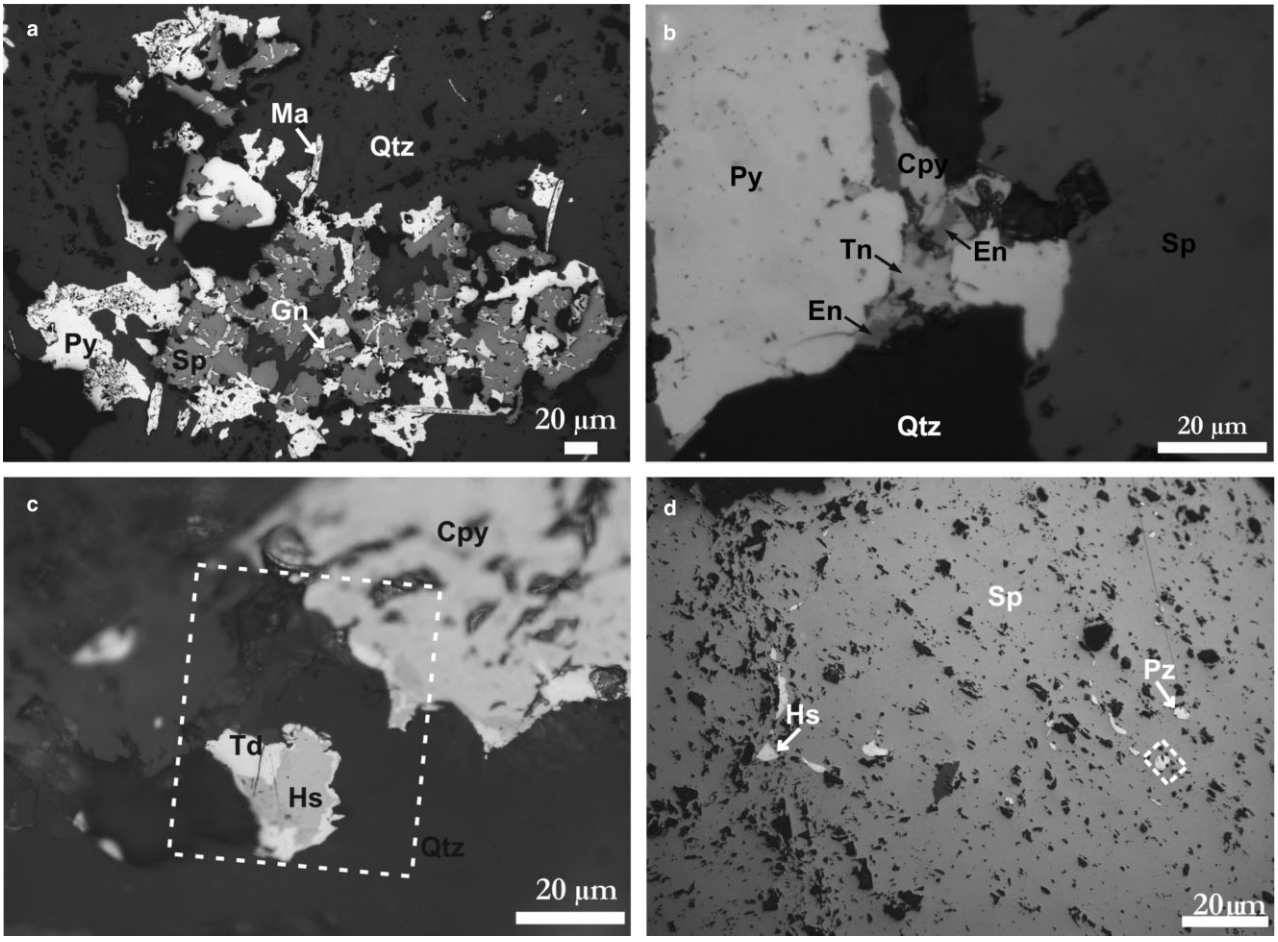

Fig. 8 Reflected light photomicrographs showing ore minerals from Arinem vein. (a) fine-crystalline galena (Gn) as veinlet in sphalerite (Sp), marcasite (Ma) intergrowth with pyrite (Py) in quartz, sample from substage IB/L440m; (b) pyrite associated with chalcopyrite (Cpy), enargite (En) replaced by tennantite (Tn) at the margin, ore minerals associated with fine-crystalline calcite and quartz, sample from substage IIC/L265m; (c) Hessite (Hs) and tetradymite (Td) as isolated crystals and inclusions in chalcopyrite, sample from substage IIA/L300m; (d) sphalerite (Sp) with inclusions of fine-crystalline hessite (Hs) and petzite (Pz), sample from substage IIC/L265m. Inset in Figure 8c, d are locations of back scattered electron image mapping (see Fig. 9).

9.4 ± 0.3 Ma). The analytical result is consistent with the regional geochronological setting of Middle–Late Miocene volcanism (Alzwar *et al*., 1992).

The occurrence of ore mineralization from the Arinem vein is more than 2000 m in length and covers a vertical range of 575 m, suggesting that the hydrothermal system was relatively large. The absence of silica sinter as a paleosurface indicator and the lack of other surface features, such as the presence of hydrothermal eruption breccias are probably due to the high rate of erosion in the region and particularly upon hydrothermal systems (Basuki *et al*., 1994). The highest grades of the gold–silver and basemetal ores occur between L440m and L200m, and the grade decreases below this depth. This limited distribution of high ore grades might have been caused by the phenomena of boiling. So far, no indication of the gold–silver supergene enrichment observed although some of the secondary copper was indicated in the very limited samples.

Based on the fluid inclusion data and presence of bladed quartz texture, in stage I boiling of hydrothermal fluid was inferred, because White and Hedenquist (1995) as well as Etoh *et al*. (2002) assumed that the bladed quartz is indicative of boiling (i.e. as pseudomorphs after bladed calcite). Subsequent cooling and

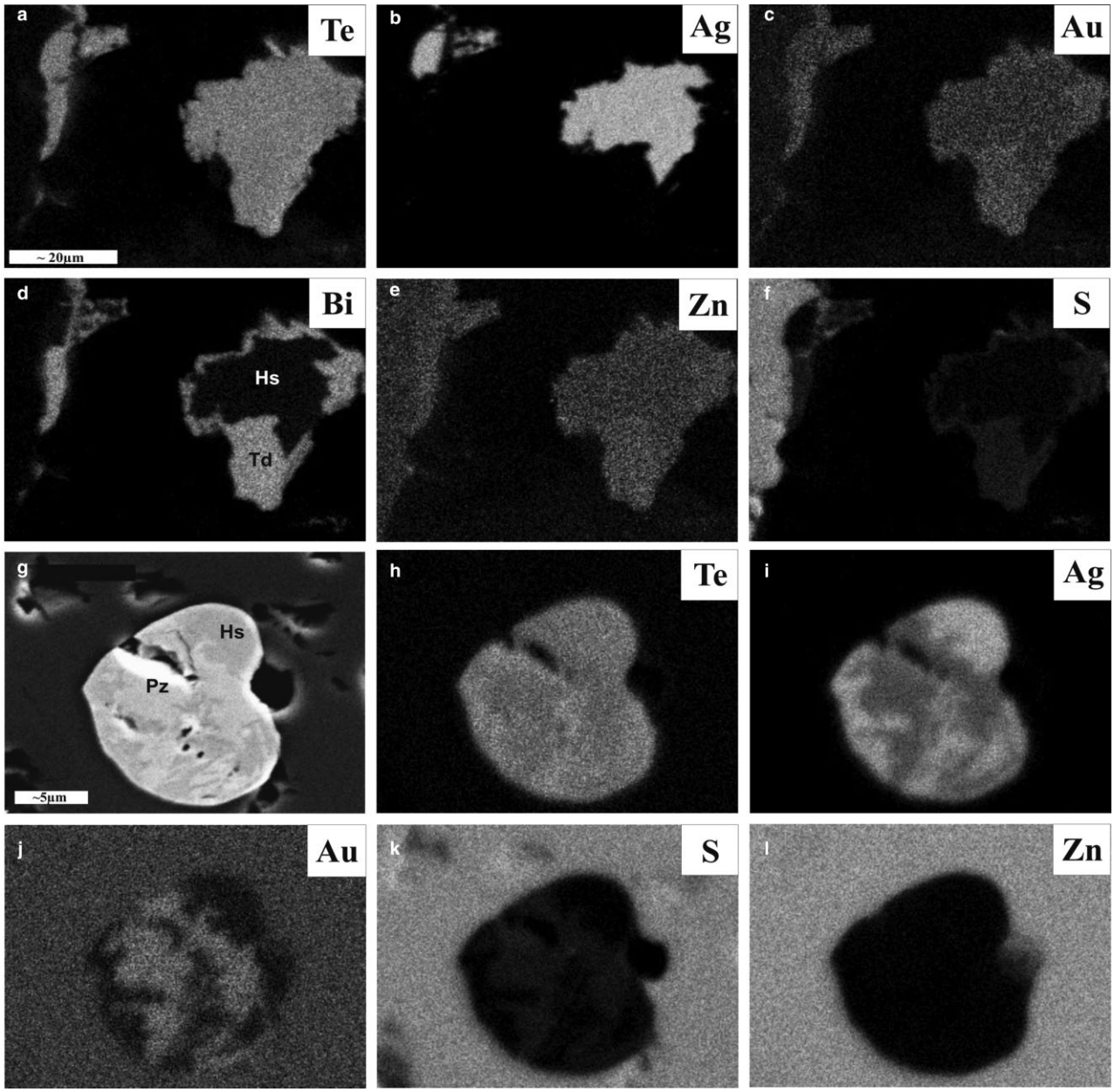

Fig. 9 (a-f): Characteristic X-ray images of Te, Ag, Au, Bi, Zn and S of tetradymite and hessite minerals, sample from substage IIA/L300m. (g) back scattered electron image showing the occurrence of hessite (Hs) associated with petzite (Pz) as inclusions in sphalerite (Sp); (h-l) characteristic X-ray images of Te, Ag, Au, S and Zn, sample from substage IIC/L265m.

the loss of H_2S into the vapor phase may have reduced the solubility of gold and caused gold precipitation above the boiling zone at stage I of mineralization. The lower temperatures and salinity obtained by microthermometry of fluid inclusions from calcite (140–217°C, 1.2–3.9 wt% NaCl equiv.) in peripheral areas to the Arinem vein might suggest that this calcite precipitated from descending fluids upon loss of CO_2 due to boiling.

Although boiling is favored in the ore depositional evidence, continuous cooling as a result of mixing with cooler meteoric water cannot be ruled out as a possible mechanism of ore deposition, at least at the late stage.

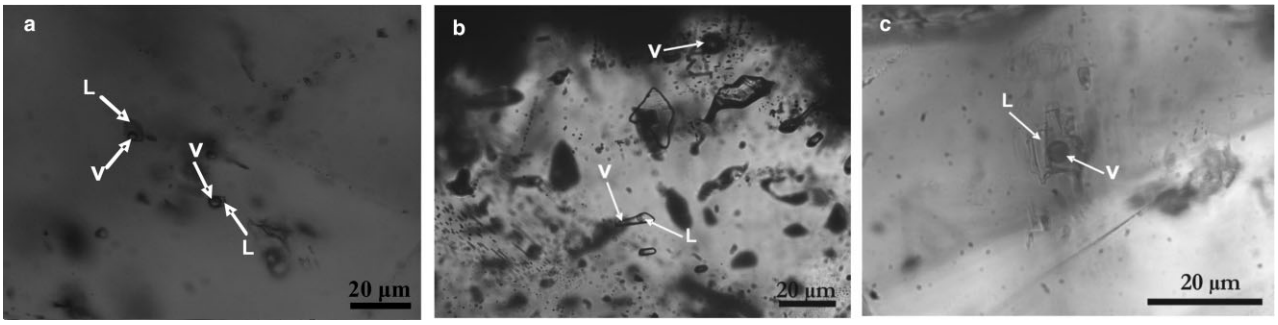

Fig. 10 Transmitted light photomicrographs (parallel nicol) of fluid inclusions trapped in quartz, sphalerite and calcite from Arinem vein. (a) two phase liquid-rich and vapor-rich fluid inclusions as cluster in coarse-crystalline quartz with variable vapor-liquid ratios/L200m; (b) two phase liquid-rich primary fluid inclusions coexisting with vapor-rich (necking) fluid inclusion trapped in sphalerite/L265m; (c) isolated two phase liquid-rich primary fluid inclusion trapped in calcite/L265m.

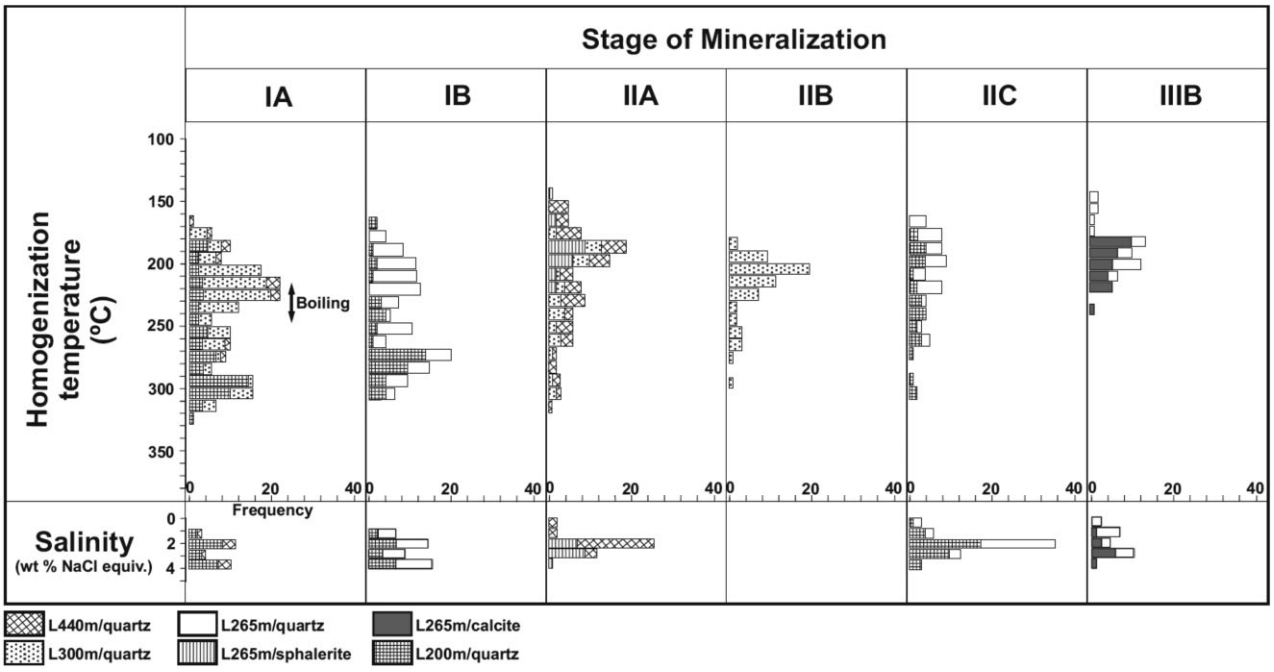

Fig. 11 Range of homogenization temperatures (top) and salinity (bottom) from fluid inclusions in main stage of mineralization (IA-IIC) and barren quartz of substage IIIB showing the slightly decrease of Th from early stage of substage IA to last stage of substage IIIB. Boiling evidence was observed in substage IA of L300m.

The association of ore minerals from the Arinem deposit is slightly different from that of the other gold deposits in western Java, for example Pongkor (Basuki *et al*., 1994; Milesi *et al*., 1999; Syafrizal *et al*., 2007; Warmada *et al*., 2007), Cirotan (Milesi *et al*., 1994), Cibaliung (Angeles *et al*., 2002; Harijoko *et al*., 2007), and Cikidang (Rosana & Matsueda, 2002). The gold mineralization ages within these other areas are mostly of Pliocene and Pleistocene age with a range from 1.5–2.1 Ma, except for Cibaliung (11.2 Ma). The gold mineralization in western Java is categorized into two different styles, there are here referred as the Pongkor and Cirotan types (Marcoux & Milesi, 1994). The Pongkor type is quartz-manganese oxide gold-bearing

veins and is characterized by low contents of sulfides with gold occurring as electrum with manganese oxides in milky quartz-calcite as gangue (Basuki *et al*., 1994; Marcoux & Milesi, 1994; Milesi *et al*., 1999). The Cirotan type is represented by quartz–rhodochrosite–polymetallic gold-bearing veins and is characterized by a high content of sulfide. The presence of Sn-bearing minerals in the Pliocene polymetallic Cirotan deposit associated with Te-bearing minerals related to the Thailand–Malaysia–Sumatra tin belt (Milesi *et al*., 1994) is quite different from the Arinem deposit, from which no Sn-bearing minerals have been observed.

The alteration, ore and gangue mineralogy of the Te-bearing Arinem deposits are typical of the quartz–illite–carbonate (low sulfidation) class of volcanic-hosted epithermal deposits. The occurrences of the sulfosalt minerals such as enargite and tennantite which overprinted the sulfide minerals at the late stage II of mineralization point to the possibility the later process become close to high-sulfidation state for the mineralization in the Arinem vein. The biggest similarity of the Arinem deposit is displayed by the Cineam deposit located about 75 km east of the Arinem. The Cineam deposit is characterized by the presence of Te-bearing minerals such as hessite, petzite and tetrahedrite-tennantite. At Cineam, the homogenization temperature of fluid inclusions from quartz are 190–240°C (some up to 350°C), the salinity is low at around 1.5–2.3 wt% NaCl equiv., and the age of mineralization is 8.0 to ~9.6 Ma (Widi & Matsueda, 1998).

7. Conclusions

The mineralized Arinem vein trends N20°E to N10°E, dips 68–83° westward over a length of about 5900 m, is 3–5 m wide and extends to a depth of 575 m. This deposit has a distinctly different ore mineral assemblage compared to those of other hydrothermal gold deposits in western Java. The Late Miocene Arinem vein deposit contains tellurium-bearing silver–gold minerals associated with abundant base metals as indicated by the occurrence of hessite, petzite, and stutzite as inclusions in sphalerite, chalcopyrite, galena, and pyrite. The Arinem deposit has characteristics of low sulfidation epithermal system with indication of high sulfidation overprinted at a later phase. The occurrence of ore mineralization over 2000 m long and 575 m deep suggests that the Arinem vein was relatively large. The mineralization age of 8.8 and 9.4 Ma is quite similar to that of the Cineam deposit in east of the Arinem deposit.

Acknowledgments

The authors are very grateful to PT. Antam Tbk of Indonesia for permission to use and publish the data, Professor Gregor Borg of the Martin-Luther University of Germany and reviewers for the valuable discussions and the correction of the earlier version of the manuscript. Our sincere gratitude to Dr. Y. Watanabe and Dr. A. Imai for editing this paper. We also thank DGHE of the Indonesia Government and FFTF Schlumberger of France for financial support.

References

Alderton, D. H. M. and Fallick, A. E. (2000) The nature and genesis of gold-silver-tellurium mineralization in the metaliferi mountains of Western Romania. Econ. Geol., 95, 495–516.

Alzwar, M., Akbar, N. and Bachri, S. (1992) Systematic geological map, Indonesia, quadrangle garut 1208-6 & Pameungpeuk 1208-3, Scale 1:100.000. Geological Research and Development Centre, 1 sheet.

Angeles, A. C., Prihatmoko, S. and Walker, J. S. (2002) Geology and alteration-mineralization characteristics of the Cibaliung epithermal gold deposit, Banten, Indonesia. Resour. Geol., 52, 329–339.

Antam (1993) Gold-silver deposit exploration report DMP, Mt. Papandayan area, Garut Regency, West Java Province (KP.DDU. 866/Jabar). Unpublished Report (in Indonesian), 68p.

Basuki, A., Sumanagara, A. D. and Sinambela, D. (1994) The Gunung Pongkor gold-silver deposit, West Java, Indonesia. Geochem. Explor., 50, 371–391.

Bodnar, R. J. (1993) Revised equation and table for determining the freezing-point depression of H_2O-NaCl solution. Geochim. Cosmochim. Acta, 57, 683–684.

Carlile, J. C. and Mitchell, A. H. G. (1994) Magmatic arcs and associated gold and copper mineralization in Indonesia. J. Geochem. Explor., 50, 91–142.

Corbett, G. J. and Leach, T. M. (1998) Southwest Pacific Rim gold-copper systems: structure, alteration, and mineralization. Soc. Econ. Geol., Special Publication, 6, 69–82.

Etoh, J., Izawa, E., Watanabe, K., Taguchi, S. and Sekine, R. (2002) Bladed quartz and its relationship to gold mineralization in the Hishikari low-sulfidation epithermal gold deposit, Japan. Econ. Geol., 97, 1841–1851.

Harijoko, A., Ohbuchi, Y., Motomura, Y., Imai, A. and Watanabe, K. (2007) Characteristics of the Cibaliung gold deposit: miocene low-sulfidation-type epithermal gold deposit in western Java, Indonesia. Resour. Geol., 57, 114–123.

Hedenquist, J. W., Izawa, E., Arribas, A. Jr and White, N. C. (1996) Epithermal gold deposits: styles, characteristics, and exploration. Soc. Res. Geol., Special Publication, 1, (poster).

Marcoux, E. and Milesi, J. P. (1994) Epithermal gold deposit in West Java, Indonesia: geology, age and crustal source. J. Geochem. Explor., 50, 393–408.

Martodjojo, S. (1982) Evolution of Bogor Basin, West Java. Institute Technology of Bandung. Unpublished PhD Thesis, 412p.

Milesi, J. P., Marcoux, E., Nehlig, P., Sunarya, Y., Sukandar, A. and Felenc, J. (1994) Cirotan, West Java, Indonesia: a 1.7 Ma hybrid epithermal Au-Ag-Sn-W deposit. Econ. Geol., 89, 227–245.

Milesi, J. P., Marcoux, E., Sitorus, T., Simanjuntak, M., Leroy, J. and Bailly, L. (1999) Pongkor (West Java, Indonesia): a Pliocene supergene-enriched epithermal Au-Ag-(Mn) deposit. Mineral. Deposita, 34, 131–149.

Rosana, M. F. and Matsueda, H. (2002) Cikidang hydrothermal gold deposit in Western Java, Indonesia. Resour. Geol., 52, 341–352.

Syafrizal, Imai, A. and Watanabe, K. (2007) Origin of ore-forming fluids responsible for gold mineralization of the Pongkor Au-Ag deposit, West Java, Indonesia: evidence from mineralogic, fluid inclusion microthermometry and stable isotope study of the Ciurug-Cikoret veins. Resour. Geol., 57, 136–148.

Van Bemmelen, R. W. (1949) The Geology of Indonesia. Government Printing Office, The Hague. IA., 732p.

Warmada, I. W., Lehmann, B., Simanjuntak, M. and Hemes, H. S. (2007) Fluid inclusion, rare-earth element and stable isotope study of carbonate minerals from the Pongkor epithermal gold-silver deposit, West Java, Indonesia. Resour. Geol., 57, 124–135.

White, N. C. and Hedenquist, J. W. (1995) Epithermal gold deposits: styles, characteristics, and exploration. Newsl. Soc. Econ. Geol., 23, 1, 9–13.

Widi, B. N. and Matsueda, H. (1998) Epithermal gold-silver-tellurides deposit of Cineam, Tasikmalaya District, West Java, Indonesia. Spec. Pub. Direct. Mineral Resour. Indonesia, 96, 1–19.